Check for updates

Advanced Materials Interfaces

ADVANCED MATERIALS INTERFACES Open Access

www.advmatinterfaces.de

RESEARCH ARTICLE OPEN ACCESS

Relationship of Dye Adsorption Onto Biomass Activated Carbon Mixed Matrix Ultrafiltration: A Mass Transfer Model Study

Khairul Anwar Mohamad Said[1,2] | Shaiza Asif[2] | Siti Zahara May Abdullah[2] | Ibrahim Yakub[2] | Harunal Rejan Ramji[2] | Md Rezaur Rahman[2]

[1]UNIMAS Water Centre, Faculty of Engineering, Universiti Malaysia Sarawak (UNIMAS), Kota Samarahan, Sarawak, Malaysia | [2]Department of Chemical Engineering and Energy Sustainability, Faculty of Engineering, Universiti Malaysia Sarawak (UNIMAS), Kota Samarahan, Sarawak, Malaysia

Correspondence: Khairul Anwar Mohamad Said (mskanwar@unimas.my)

Received: 25 September 2025 | **Revised:** 26 January 2026 | **Accepted:** 17 March 2026

Keywords: driving force of mass transfer | dye rejection | film mass transfer | flux | global mass transfer | polyvinylidene fluoride

ABSTRACT

The purpose of this study was to investigate the adsorption of dye molecules from water resources, with a particular emphasis on the use of activated carbon as an adsorbent in polymer membranes to purify low-quality waters to produce clean water. Polyvinylidene fluoride (PVDF) membranes' removal efficiency was substantially enhanced by the initial concentration of 10 ppm methylene blue (MB). 1.07 ppm of MB was present in the pristine membrane, resulting in a removal efficiency of 89.29%. The removal efficacy was observed to increase to 96.34% when PVDF membranes were incorporated with biomass-activated carbon (BAC). Removal efficiency is substantially determined by the initial concentration of the adsorbate solution. The initial concentration of 0.5 mg/L resulted in the removal of nearly 100% of MB. The modification of the mass transfer model proposed has the broadest applicability in determining the resistance of mass transfer for the adsorption process. In relation to the adsorption of dye onto biomass-activated carbon, the influence of surface area occupation is driven by film mass transfer. The importance of the role of surface area occupation in modulating the resistance of mass transfer in the adsorption is emphasized by the fact that the film mass transfer increased as the driving force of mass transfer (C-C*) increased.

1 | Introduction

Some of the toxic pollutants that come from various sources, including fabric, cosmetic, paper, pharmaceutical, and dyestuff manufacturing industries, are dyes [1]. These industries use colorants in their processes and generate aromatic dye wastewater containing benzene rings, including methylene blue [2]. Discharging colored wastewater into the environment may result in aesthetic pollution, eutrophication, and disturbances to aquatic life, as indicated by [2]. Methylene blue, an extensively used cationic colorant, exhibits environmental persistence and possesses toxic, carcinogenic, and mutagenic properties [3]. Extended contact with methylene blue can hint at notable health concerns, involving anemia, tumors, nausea, eye rash, vomiting, and psychological confusion [2]. Consequently, to prevent environmental and health hazards, it is necessary to treat wastewater containing methylene blue and other dyes.

Currently, methods for treating dye wastewater primarily encompass chemical precipitation, ozonation, photolysis, adsorption, and membrane separation techniques [4]. Due to their price-effectiveness and eminent efficacy, film separation techniques and adsorption techniques are broadly utilized in effluent management. Common membrane separation techniques include

This is an open access article under the terms of the Creative Commons Attribution License, which permits use, distribution and reproduction in any medium, provided the original work is properly cited.

© 2026 The Author(s). *Advanced Materials Interfaces* published by Wiley-VCH GmbH

nanofiltration (NF) and ultrafiltration (UF). NF, while effective, entails elevated treatment expenses when dealing with low-concentration and extensive volumes of dye wastewater, primarily because of its comparatively high operational pressure. In contrast, UF operates at a lower pressure, rejecting contaminants larger than the size of the membrane pores, although it is less effective for removing smaller pollutants like small molecular organic dyes [5].

The adsorption technique involves the introduction of an adsorbent into dye wastewater, which physically or chemically adsorbs dye molecules onto its surface. Activated carbon, derived from natural, inexpensive waste materials like branches, seashells, tea leaves, roots, coconut husk, and shoots, is the frequently employed adsorbent substance. Activated carbon is commonly employed as an adsorptive material because of its chemical stability and well-developed porosity; however, its commercial production is often associated with relatively high costs. Consequently, recent research has increasingly focused on valorising low-cost biomass residues as alternative carbon sources within sustainable and circular material frameworks. For example, agro-industrial by-products such as brewer spent grain have been converted into functional carbon materials through multi-step activation routes, yielding activated carbon and carbon nanotubes with promising performance (Ahmed et al., 2019) In another approach, herbaceous biomass treated under alkaline conditions has been reported to produce carbon nanomaterials with exceptionally high surface areas, reaching up to 1368 $m^2\ g^{-1}$ (Osman et al., 2020)Utilizing natural waste for activated carbon production enhances economic value and diminishes expenses, serving as a standard alternative to conventional activated carbon [6]. However, a notable challenge is that activated carbon adsorbents are typically prepared as powders and introduced into the water, incurring significant economic costs for the process of isolating the adsorbent material. Additionally, in large-scale operations, inevitable losses of adsorbents can occur, potentially posing a detrimental impact on water bodies due to the loss of powdered activated carbon material [6].

Adsorption has emerged as a prominent method for the isolation of trace aquatic contaminants owing to its simplicity, efficiency, and versatility [7]. Nonetheless, certain limitations and bottlenecks persist, including a sluggish pace and significant internal diffusion resistance in the adsorbent that require resolution. Consequently, further efforts have been focused on discovering cost-effective and efficient water technologies to address the constraints. This transitions the emphasis from traditional adsorption to adsorptive membranes, which may eliminate various harmful contaminants that significantly endanger human health and the environment. The merger of adsorption and membrane technology, as indicated by its name, is among the most promising solutions [8]. The utilization of adsorptive membranes provides answers to several challenges, including membrane fouling, elevated energy usage, regeneration expenses, and selectivity issues. In comparison to traditional filtering membranes, adsorptive membranes offer enhanced contaminant ion retention, reduced energy usage, and improved permeate flow. The operational procedure of membranes can be extended beyond mere filtering to encompass adsorption. Furthermore, its separation rate surpasses that of traditional adsorptive beads, since the eliminated contaminant ions may be conveyed by convective flow to both exterior and interior binding sites, rather than relying on the sluggish diffusion to either site [9]. By simultaneously executing adsorption and filtration, the adsorptive membrane enables a mass transfer mechanism in which the target pollutant is transported to the solid surface through physicochemical interactions through a porous membrane medium. This process requires minimal energy consumption and low pressure. Nanofiltration and reverse osmosis, which are the most common membrane separation methods for eliminating identical contaminants, may require membranes that are extraordinarily dense, resulting in significant energy consumption. The adsorbents can be replenished through desorption, which is a reversible process. Their efficacy is contingent upon the morphology and specific contaminants that they target [10].

Despite its technological advantages, this approach possesses intrinsic limitations, including agglomeration and expensive processes associated with adsorbent in granular form. Consequently, current research has increased to create economical adsorbents [10]. Adsorptive membrane technology can eliminate various pollutants from wastewater owing to its diverse conformations, extensive surface area, ample adsorption sites, and varied fillers [7]. The incorporation of polymers and/or particles with a strong affinity for metal ions and molecules into the membrane enhances its technological capabilities by facilitating low operating pressure, high permeability flux, regeneration, recyclability, and compact size [7]. Recent studies have demonstrated that integrating life cycle assessment (LCA) into materials development is essential for evaluating the environmental impacts of the entire process, from waste-derived feedstock selection to material synthesis, application, and recyclability. For example, Osman et al. (2022) demonstrate the sustainable synthesis of a magnetic char composite derived from plastic bottle waste as polyethylene terephthalate (PET) and biomass. A life cycle assessment (LCA) was conducted to evaluate the environmental impacts of the entire preparation process, with abiotic depletion of fossil fuels and global warming potential quantified as 7.17 MJ and 0.63 kg CO_2, respectively, for one functional unit (1 kg of pomace leaves). The resulting composite exhibited excellent crystal violet (CV) dye removal performance, with magnetic properties enabling efficient separation and high removal efficiency across a wide pH range due to pore filling, hydrogen bonding, and π–π interactions, best described by the Langmuir isotherm model. Overall, this work highlights the importance of coupling material performance with full-process LCA to support the development of sustainable, waste-derived sorbents aligned with circular economy principles, with future studies focusing on real wastewater and large-scale applications (Osman et al., 2022).

For example, thermal plasma synthesis, sol-gel synthesis, flame synthesis, electrodeposition, ion sputtering, and mechanical milling/alloying are all methods that are used to produce inorganic fillers, in contrast to mixed matrix membranes that contain organic fillers. These inorganic additives are covalently bonded to the membrane matrix through hydrogen bonds or van der Waals interactions. The membrane functionality is improved by the utilization of numerous additives. At an initial concentration of 5 mg/mL, the dye rejection rate was enhanced to 82.3% by the incorporation of zinc oxide (ZnO) into the polyethersulfone (PES) matrix [11]. Nearly total dye elimination was effectively

21967350, 0, Downloaded from https://advanced.onlinelibrary.wiley.com/doi/10.1002/admi.202500888 by National Institutes Of Health Malaysia, Wiley Online Library on [06/04/2026]. See the Terms and Conditions (https://onlinelibrary.wiley.com/terms-and-conditions) on Wiley Online Library for rules of use; OA articles are governed by the applicable Creative Commons License

accomplished when the graphene oxide (GO) was included in the PES matrix as nanoplates [12]. The enhanced performance of this membrane was ascribed to the presence of an acidic functional group on its surface, which eventually augmented the membrane's hydrophilicity. This characteristic improved the permeability and selectivity of the membrane [13]. Recent work on biochar adsorbents highlights the high capacitive uptake of pharmaceutical pollutants under competitive conditions. For instance, olive tree pruning biochar achieved removal efficiencies >95% for both promazine and promethazine from binary mixtures, with maximum adsorption capacities up to 640.7 and 346.95 mg g^{-1}, respectively, following Langmuir–pseudo-second-order behaviour and stable regeneration over multiple cycles (El-Azazy et al., 2023). These findings emphasize how surface functionality and accessible porosity control uptake in biochars, and provide a useful benchmark for interpreting the sorptive performance of BAC in the present membrane context.

Numerous models and theories that have been formulated are applicable to certain objectives [14, 15]. The mass transfer factor models established by Ref. [16] are applicable for assessing the mass transfer resistance during the adsorption of a single solute onto granular activated carbon (GAC) from an aqueous solution. Given that surface water comprises many solutes, the presented models [16] are inadequate for elucidating the mechanisms of competitive adsorption of multiple solutes, which are significantly more intricate than those involving a single solute.

Since the high concentrations of this solute in water resources present challenges for conventional treatment methods for potable water, the objective of this research endeavour was to conduct a comprehensive, systematic examination of the adsorption of dye molecules. This research was conducted with the primary objective of improving comprehension of solute adsorption and its importance in the removal of dye molecules from surface water. Specifically, it focused on the utilization of activated carbon as an adsorbent in polymer membranes for the purification of low-quality waters for clean water production.

2 | Methodology

2.1 | Materials

Powdered activated carbon derived from pine wood was synthesized in-house. Polyvinylidene fluoride (PVDF), N-methyl pyrrolidone (NMP, 99.5%), Lithium Chloride, and methylene blue (MB, 98%) were sourced from Sigma–Aldrich.

2.2 | Membrane Fabrication

The cast film solutions were formulated with a uniform concentration of 15 wt.% PVDF and 4 wt.% lithium chloride. The solvent concentration in the casting solution was adjusted based on the biomass-activated carbon (BAC) content. Different quantities of BAC, as shown in Table 1 below, were included in the casting solution.

A homogenous suspension was obtained by concurrently combining all components with NMP and agitating the mixture with a magnetic stirrer at 400 rpm for 24 h. Thereafter, the mixture was applied to the glass plate utilizing a casting rod with a thickness of 250 μm. The wet cast film underwent a solvent/non-solvent exchange procedure in a water bath. The successive films were ultimately preserved in deionized water at ambient temperature.

2.3 | Characterization

The functional group was analyzed by investigating the membrane at wavelengths ranging from 4000 to 400 cm^{-1} using Fourier transform infrared spectroscopy (FTIR). The cross-sectional and surface images of the membranes were obtained using scanning electron microscopy (SEM). To preserve the cross-sectional structure during the fracture, liquid nitrogen was employed to excise small membrane fragments. Afterward, the minced portion was dried in an oven at 60°C for 2 h to eliminate moisture from the membrane pore. The membrane samples were coated with gold-platinum prior to analysis to enhance the electron conductivity across the membrane surface.

The Brunauer–Emmet–Teller (BET) pore size analyzer is an essential tool for measuring the surface characteristics and pore properties of BAC particles. The BET theory expands the Langmuir theory of monolayer adsorption to encompass multilayer adsorption. The process is quantifying the volume of gas (nitrogen) adsorbed onto a material at varying relative pressure to ascertain the specific surface area. The BET surface area analysis was conducted according to the ASTM D6556-14 (2014) standard. The degassing temperature was set at 130°C for 3 h. The test was repeated numerous times for each sample, and the most representative results were selected.

The specific surface area was determined by analyzing the gas adsorption isotherms, which graph the volume of gas adsorbed with the relative pressure. A particle size analyzer (PSA) is essential for measuring the particle size distribution in BAC particles. Comprehending the particle size distribution was crucial as it influences the material surface area, porosity, adsorption capacity, and overall efficacy in diverse applications. The analysis of data in PSA involved the particle size distribution curve, cumulative distribution, and statistical curve, visually depicting the frequency of various particle sizes within the sample. The cumulative distribution illustrated the proportion of particles beneath a specified size, which was beneficial for comprehending the dispersion and consistency of particle sizes. Statistical indicators, including mean particle size, median particle size, and standard deviation, facilitated the summarization of particle size distribution.

The analysis of water absorption measurement was employed to quantify the water content in the membrane by contrasting the weights in both dry and wet states. The membrane sheets were sectioned into squares of 3×3 cm^2 and desiccated in an oven for 24 h. The weight was documented post-drying. Subsequently, an identically sized membrane was immersed overnight in distilled water at ambient temperature. Subsequently, the surplus moisture was removed using blotting paper prior to reweighing. The

21967350, 0, Downloaded from https://advanced.onlinelibrary.wiley.com/doi/10.1002/admi.202500888 by National Institutes Of Health Malaysia, Wiley Online Library on [06/04/2026]. See the Terms and Conditions (https://onlinelibrary.wiley.com/terms-and-conditions) on Wiley Online Library for rules of use; OA articles are governed by the applicable Creative Commons License

TABLE 1 | Membrane compositions.

Sample	PVDF (wt.%)	Lithium chloride (wt.%)	BAC (wt.%)	NMP (wt.%)
PVDF	15	4	0	81.00
PVDF-BAC-0.05	15	4	0.05	80.95
PVDF-BAC-0.10	15	4	0.10	80.90
PVDF-BAC-0.15	15	4	0.15	80.85
PVDF-BAC-0.20	15	4	0.20	80.80

water absorption was determined as follows:

$$Water\ uptake = \frac{W_{wet} - W_{dry}}{Wdry} \times 100\% \quad (1)$$

where W_{wet} represents the mass of the dry membrane, W_{dry} denotes the mass of the dehydrated membrane.

The membrane porosity was examined to assess the impact of mixing the BAC particles on the membrane pore size by a gravimetric approach utilizing the subsequent equation:

$$\varepsilon = \frac{W_{wet} - W_{dry}}{\rho_{water} \times A \times L} \times 100\% \quad (2)$$

A represented the effective area of the membrane, whilst L denoted the thickness of the membrane, ρ_{water} signifies the density of water (0.998 g/cm^3). The membrane thickness was measured using a micrometer.

2.4 | Membrane Performance

The water permeate flow was the primary metric used to assess the efficacy of ultrafiltration membranes. The membrane active separation area was 20 cm^2, and the precise measuring technique involved pre-pressurizing the membrane at 0.15 MPa for 30 min. Subsequently, the water flux stabilized, and the pressure was adjusted to 0.1 MPa. The following formula was employed to ascertain the absolute water flux (J_0):

$$J_0 = \frac{V}{A\Delta t} \quad (3)$$

In the given formula, J_0 signifies the pure water flux (L/m.h^2); V indicates the permeate volume (L); A represents the effective membrane area; and Δt shows the filtration duration (h).

The impact of an initial 10 mg/L concentration of methylene blue dye was examined. To attain adsorption equilibrium, 0.2 g of the film was immersed in varying concentrations of methylene blue (0.5, 2, 5, and 7 ppm) and allowed to adsorb undisturbed for one day. The corresponding concentrations were determined by evaluating the absorbance of methylene blue prior to and during adsorption at 668 nm using a UV–vis spectrophotometer. The adsorption capacity of the PVDF membrane integrated with BAC was ascertained by employing the following formula:

$$q_e = \frac{(C_0 - C_e)V}{m} \quad (4)$$

In the given formula, q_e denotes the adsorption capacity (mg/g), C_0 signifies the initial concentration of MB (mg/L), C_e represents the concentration of MB at equilibrium (mg/L), V indicates the volume of the solution (L), and m refers to the mass of BAC (mg). The BAC mass was calculated from the nominal BAC weight fraction in the casting dope and the dry membrane mass (0.2 g), assuming homogeneous dispersion within the polymer matrix.

To evaluate the actual operational performance of the BAC adsorption ultrafiltration membrane, MB at a concentration of 0.5 ppm was introduced at designated flow rates utilizing a laboratory filter device. Permeate samples were obtained at 100-s intervals. The concentration of methylene blue was measured before and after filtering using a UV–vis spectrophotometer. The removal effectiveness of methylene blue by the membrane was calculated using the following formula:

$$R = \frac{(C_0 - C_e)}{C_0} \times 100\% \quad (5)$$

In the equation, R represents the percentage of MB elimination, C_0 denotes the starting concentration of MB in ppm, and C_e indicates the concentration of MB at equilibrium in ppm.

2.5 | Numerical Simulation

The mass transfer equation that characterizes the adsorption processes of mixtures onto porous materials from contaminated water should be resolved using approximation approaches. This work uses the following formula [16, 17] as the foundation for subsequent equations, which will elucidate the mass transfer mechanism during the adsorption of dye molecules onto activated carbon in membranes from contaminated water as follows:

$$\ln\left(\frac{C_0}{C_s}\right) = [k_L a]_f \cdot t \quad (6)$$

where C_0 represents the concentration of the solute entering the membrane (mg/L), C_s denotes the concentration of the solute exiting the membrane (mg/L), k_L is the mass transfer coefficient (m/h), a signifies the surface area of the interfacial liquid–solid (1/m), $[k_L a]_f$ refers to the film mass transfer factor, external mass transfer factor, or volumetric film mass transfer coefficient (1/h), and t indicates the accumulation time (h).

Equation (7) implies that the relationship between global and external mass transmission may be reformulated as:

$$[k_L a]_f = [k_L a]_g \times e^{-\beta \times \ln(q)} \quad (7)$$

21967350, 0, Downloaded from https://advanced.onlinelibrary.wiley.com/doi/10.1002/admi.202500888 by National Institutes Of Health Malaysia, Wiley Online Library on [06/04/2026]. See the Terms and Conditions (https://onlinelibrary.wiley.com/terms-and-conditions) on Wiley Online Library for rules of use; OA articles are governed by the applicable Creative Commons License

where [kLa]g is the global mass transfer coefficient (1/h), β is the adsorbate–adsorbent affinity parameter (g.h/mg), and q is the cumulative quantity of solute adsorbed onto activated carbon (mg/g). The updated mass transfer model, which is a continuous equation (refer to Equation 8), is obtained by incorporating Equation (7) into Equation (6). This equation can be used to calculate the fluctuation of the global mass transfer factor in relation to the C_0/C_s ratio. The revised model of Equation (8) is applicable to the adsorption of one or more solutes onto activated carbon from polluted water and necessitates validation through experimental data, as outlined below:

$$\ln\left(\frac{C_0}{C_s}\right) = [k_L a]_g \times e^{-\beta \times \ln(q)} \times t \tag{8}$$

Rearranging the Equation (8) yield the linear expression of:

$$\ln(q) = B + \frac{1}{\beta} \times \ln(t) \tag{9}$$

$$B = \frac{ln\left([k_L a]_g\right) - \ln\left(\ln\left(\frac{C_0}{C_s}\right)\right)}{\beta} \tag{10}$$

B is the potential mass transfer index associated with the driving force of mass transfer (mg/g).

The porosity diffusion factor is defined as the disparity between the global and film mass transfer factors. This can be expressed in an equation as follows:

$$[k_L a]_d = [k_L a]_g - [k_L a]_f \tag{11}$$

$[k_L a]_d$ represents the porous diffusion factor or the internal mass transfer coefficient (1/h). Employing Equation (11) enables the calculation of the values for variable $[k_L a]_d$ based on the C_0/C_s ratio, as the fluctuation of $[k_L a]_g$ and $[k_L a]_f$, ascertained by Equations (10) and (7) respectively, was validated. The revised mass transfer factor models in Equations (7–9) can effectively forecast the mass transfer resistance for the adsorption of species such as dye molecules onto activated carbon.

3 | Results and Discussion

3.1 | Physicochemical Properties

FTIR analysis was conducted to determine the chemical properties of functional groups of BAC powder and different PVDF membranes, as exemplified in Figure 1. The functional group and its quantified frequencies were compared with the data gathered by Nandiyanto, Oktiani, & Ragadhita (2019) (Nandiyanto et al., 2019). The FTIR results reveal the presence of various functional groups, each of which is responsible for the adsorption of O—H, C—H, C═O, C—O, and C—F (Table 2). According to the FTIR results, the synthesized BAC particles indicated the presence of a hydroxyl group (O—H stretching) at around 3741.90–3738.05 cm^{-1}. This indicates the presence of hydroxyl groups, which are known for their hydrophilic properties and potential to form hydrogen bonds. The PVDF membranes have a characteristic peak representing the stretching vibrations of C—H bonds in alkyl groups at around 3367.71–3329.14 cm^{-1}. These peaks are typical for aliphatic C—H stretching vibrations. It was observed at peaks around 1643.35–1639.49 cm^{-1} suggesting that there was a carbonyl group (C═O). These groups can be present in ketones, aldehydes, or carboxylic acids, contributing to the chemical complexity of the material. C—O stretching was visible at a peak 1400.32 cm^{-1} from carboxyl and alcohol groups, further enhancing the hydrophilic nature of the membrane. Characteristics of C—F bonds in the PVDF structure were detected at 1172.72 cm^{-1}. The presence of fluorine contributes to the chemical stability and hydrophobicity of the PVDF membrane. By analyzing these peaks, it was confirmed that there was the presence of both PVDF and BAC in the membranes. The functional groups from the BAC provided additional characteristics, enhancing the membranes' properties. The inclusion of BAC within the PVDF membrane matrix resulted in the appearance of a large number of hydrophilic hydroxyl and carboxyl functional groups on the PVDF membrane surface. These groups have the potential to improve the water permeability of the membrane, and their role will be examined in depth in a later part of the discussion.

The SEM imaging indicates the pores of the pristine and PVDF-BAC-0.2 membrane are uniformly distributed throughout the membrane surface, with diameters in the tens of nanometers, consistent with the usual pore sizes of ultrafiltration membranes. Cross-sectional SEM images (Figure 2) show that the pristine PVDF membrane exhibits a typical asymmetric structure with large finger-like macrovoids, whereas incorporation of 0.2 wt.% BAC leads to partially suppressed and more elongated macrovoids with a relatively denser top skin layer. These morphological changes are consistent with the quantitatively updated porosity results, indicating moderated phase-inversion kinetics upon BAC addition. The resulting interconnected pore structure reduces transport resistance, explaining the enhanced permeate flux while maintaining high dye rejection (> 90%). This signifies that the BAC powder is an appropriate adsorbent material. Research by Li, Luo, and Li [18] indicates that the specific surface area and pore volume of the PSF membrane were greater than those of the PSF membrane with 0.1% BAC, whilst the pore size has diminished [18]. The study also indicated that the incorporation of BAC powder into the mixed matrix membrane resulted in a slightly protruded membrane surface, a phenomenon due to the high viscosity of the membrane casting solution.

The SEM was used to analyze the cross-section of the membranes at various loadings at a magnification of 20 kX, as illustrated in Figure 2.

The solvents NMP and water exhibited a high affinity, resulting in a unique layered membrane structure that included a dense top epidermis layer, a porous sub-layer, and a sponge-like bottom layer. In Figure 2, the incorporation of BAC into the matrix membrane was observed to restrict the formation of finger-like macropores during the phase inversion process when compared to the pristine PVDF membrane and the PVDF-BAC-0.2 membrane. Additionally, the PVDF membrane with BAC addition contained more finger-like pores at the top, unlike the larger pores at the bottom. This BAC-induced pore structure is

21967350, 0, Downloaded from https://advanced.onlinelibrary.wiley.com/doi/10.1002/admi.202500888 by National Institutes Of Health Malaysia, Wiley Online Library on [06/04/2026]. See the Terms and Conditions (https://onlinelibrary.wiley.com/terms-and-conditions) on Wiley Online Library for rules of use; OA articles are governed by the applicable Creative Commons License

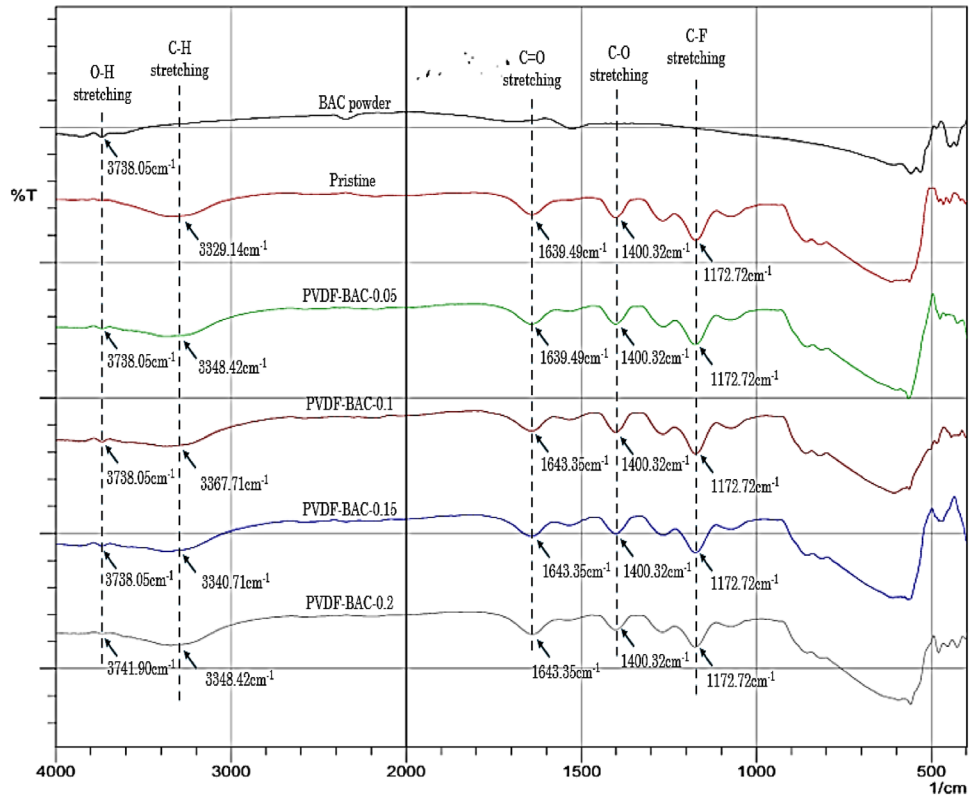

FIGURE 1 | FTIR analysis of BAC, pristine, and modified membranes.

TABLE 2 | FTIR interpretation of BAC, pristine, and modified membrane.

Sample	Characteristic peaks (cm^{-1})	Chemical bonds	Assigned functional groups
BAC powder	3738	O—H stretching	Hydroxyl groups
Pristine PVDF membrane	3329, 1639, 1400, 1173	C—H, C=O, C—O, C—F stretching	Alkyl, carbonyl, carboxyl/alcohol, PVDF backbone
PVDF–BAC-0.05 membrane	3738, 3348, 1639, 1400, 1173	O—H, C—H, C=O, C—O, C—F stretching	Hydroxyl (BAC), alkyl, carbonyl, carboxyl/alcohol, PVDF backbone
PVDF–BAC-0.1 membrane	3738, 3368, 1643, 1400, 1173	O—H, C—H, C=O, C—O, C—F stretching	Hydroxyl (BAC), alkyl, carbonyl, carboxyl/alcohol, PVDF backbone
PVDF–BAC-0.15 membrane	3738, 3341, 1643, 1400, 1173	O—H, C—H, C=O, C—O, C—F stretching	Hydroxyl (BAC), alkyl, carbonyl, carboxyl/alcohol, PVDF backbone
PVDF–BAC-0.2 membrane	3742, 3348, 1643, 1400, 1173	O—H, C—H, C=O, C—O, C—F stretching	Hydroxyl (BAC), alkyl, carbonyl, carboxyl/alcohol, PVDF backbone

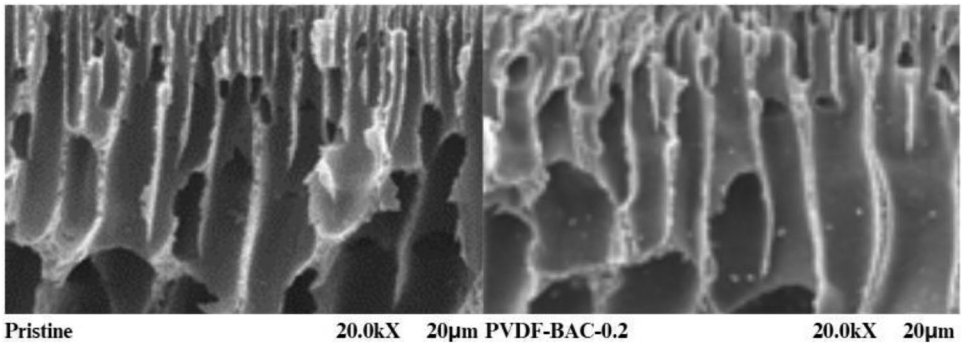

FIGURE 2 | SEM images for the cross-sectional area of pristine and PVDF-BAC-0.2 membranes.

21967350, 0, Downloaded from https://advanced.onlinelibrary.wiley.com/doi/10.1002/admi.202500888 by National Institutes Of Health Malaysia, Wiley Online Library on [06/04/2026]. See the Terms and Conditions (https://onlinelibrary.wiley.com/terms-and-conditions) on Wiley Online Library for rules of use; OA articles are governed by the applicable Creative Commons License

TABLE 3 | BET interpretation for BAC powder.

Surface area (m^2/g)	Pore size (A)	v_{pore} (cc/g)	Relative pressure (P/P_0)	r_{pore} (A)
410.686	2.54008	0.5216	0.99476	< 1836.9

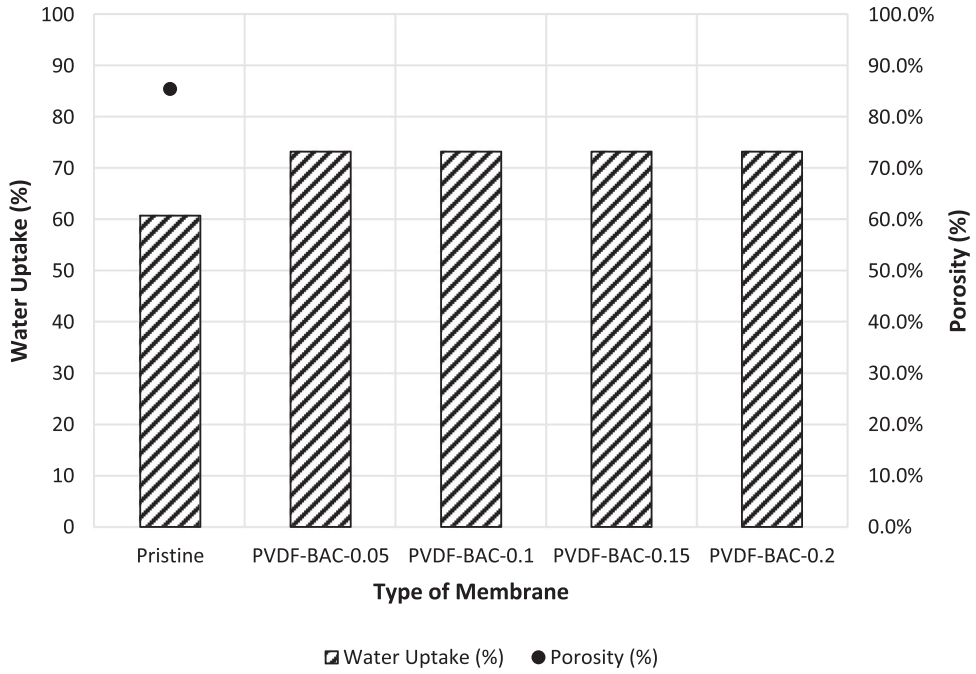

FIGURE 3 | Water uptake and porosity of pristine and modified membrane.

advantageous for reducing mass transfer resistance and improving membrane flux [18]. Compared to the pristine membrane, the PVDF-BAC-0.2 membrane possessed a greater pore size diameter.

The surface area, pore size, and pore volume of the BAC were determined using the Brunauer-Emmett-Teller (BET) isotherm method, as presented in Table 3.

The adsorption and desorption isotherm for the BAC sample is presented in Figure S1. The isotherm exhibits a characteristic type-III shape, with a distinct hysteresis loop. Type III isotherms are indicative of weak interactions between the adsorbent and adsorbate (Zhang, et al., 2016). The hysteresis noted in the adsorption/desorption isotherm was ascribed to capillary condensation in the mesoporous structure of the sample. The sample demonstrated capillary condensation, accompanied by a broad hysteresis loop. The BAC sample exhibited a Type-H3 isotherm, indicative of the tensile strength effect. The configuration of these curves indicates the existence of tiny-slit mesopores in the material.

The water absorption capabilities were measured to evaluate the wettability quality of synthesized membranes with varying composition of BAC, as illustrated in Figure 3. The immaculate PVDF membrane exhibits a water absorption of 60.78%. The PVDF membrane integrated with BAC exhibited a comparable water absorption of 73.27%, showing no significant variation from the decreased BAC weight level of each membrane. This revealed that the incorporation of BAC into the membrane matrix enhances the membrane absorption of water molecules due to BAC's hydrophilic properties. Additionally, the porosity of the pristine membrane was measured at 0.85%, while the membranes with the greatest porosity, PVDF-BAC-0.15 and PVDF-BAC-0.2, had a porosity level of 72%–75%. The uniformity in porosity indicated that the structural integrity and pore dispersion of the PVDF membrane were not substantially affected by the incorporation of BAC. The increased water absorption is probably attributable to the inherent characteristics of the BAC.

3.2 | Membrane Performance Study

Table 4 compares the separation performance of the PVDF–BAC mixed-matrix membrane developed in this work with previously reported PVDF-based mixed-matrix membranes incorporating carbonaceous, metal-oxide, and MOF fillers for dye removal. Key performance parameters, including operating pressure, permeate flux, dye rejection, and stability over various filtration cycles, are benchmarked under comparable analytical conditions. The results highlight the relative position of the present membrane with state-of-the-art published literature. A detailed discussion of the influence of each parameter on membrane performance is provided in the subsequent sections based on the findings of this study.

21967350, 0, Downloaded from https://advanced.onlinelibrary.wiley.com/doi/10.1002/admi.202500888 by National Institutes Of Health Malaysia, Wiley Online Library on [06/04/2026]. See the Terms and Conditions (https://onlinelibrary.wiley.com/terms-and-conditions) on Wiley Online Library for rules of use; OA articles are governed by the applicable Creative Commons License

TABLE 4 | Performance of the PVDF–BAC mixed-matrix.

Membrane system	Polymer	Filler (loading)	Dye	Feed concentration ($mg\ L^{-1}$)	Operating pressure (bar)	Flux ($L\ m^{-2}\ h^{-1}$)	Rejection (%)	Stability/cycles	Reference
PVDF–BAC	PVDF	BAC (0.2 wt.%)	MB	10	1	Enhanced versus pristine	>90	Stable (5 cycles)	This work
PVDF–GO MMM	PVDF	Graphene oxide (0.1 wt.%–0.5 wt.%)	MB	10	1	120–180	95–99	3–5 cycles	(Ntone et al., 2026)
PDA@ZnO/PVDF	PVDF	PDA-coated ZnO	DB-70	50	1	1339 (pure water)	88.5	Multiple	(Zhai & Yang, 2023)
PVDF/Ag-ZnO	PVDF	ZnO 5 wt.%, trace amount Ag	RB5	10	1	192	N/A	3 cycles	(Chamam et al., 2025)
PVDF–UiO-66-NH_2 MMM	PVDF	RhB, CR	MB	N/A	1	231.6	96.4,98.3	5 cycles	(Ghomi, 2024)

3.3 | Water Flux

Figure 4 shows the collected pure water (mL) over time (seconds) for different PVDF membranes with various weight percentages. The pristine PVDF membrane has the lowest slope, indicating the smallest pure water flux. The PVDF-BAC-0.2 has the steepest slope, indicating the greatest pure water flux among the tested films.

Figure 5 illustrates the water flux of pristine and modified PVDF membranes, demonstrating that the water flux is enhanced with a rise in the weight content of BAC incorporated into the PVDF membrane. The water flow of the PVDF-BAC-0.2 membrane, which contains 0.2 wt.% BAC, is 426 $L/m^2.h$, indicating an approximate 50% enhancement relative to the pristine membrane. This obviously supports the conclusion of Yang et al. (2023) that the integration of BAC into membranes improves their permeability. The increased water flux is a result of the PVDF membrane's increased porosity and hydrophilicity, which are a direct result of the addition of BAC. Nevertheless, the viscosity of the casting solution increases as the BAC concentration increases, which may result in BAC agglomeration and the restriction of macropore development. Transmembrane resistance is increased as a consequence of the reduction in transmembrane channels for water molecules. In comparison to the unadulterated membrane, the membranes that were incorporated with BAC exhibited a higher degree of hydrophilicity and porosity, which facilitated a more efficient passage of water.

3.4 | Solute Flux

Figures 6 and 7 illustrates the volume of collected filtered solute with time for each PVDF membrane during the filtration of a 10 mg/L methylene blue (MB) solution. The pristine membrane has the lowest slope, signifying that it required a longer duration to accumulate 100 mL of filtered solute, thus demonstrating that the pristine PVDF membrane has lower permeability. The PVDF-BAC-0.05 membrane exhibited a steeper slope relative to the pristine membrane, signifying a modest increase in solute accumulation throughout each time interval. The incorporation of a small quantity of BAC into each membrane enhances its permeability. It is noteworthy that the volume of water collected throughout each time interval when filtering the MB solute was smaller than that obtained when filtering water.

Figure 7 provided a quantitative comparison of the membrane flux for each PVDF membrane when filtering the 10 mg/L MB solution. The pristine membrane had a flux of 179.323 $L/h/m^2$. This low value indicates limited permeability to the MB solution, suggesting that the unmodified PVDF membrane was not effective for filtering the MB solute. However, when BAC was introduced to the membrane, the flux improved, which indicated that the increasing BAC weight composition further enhanced the membrane's ability to filter the MB solution. The solute flux in Figure 8 is lower than the pure water flux in Figure 7, indicating a reduction in permeability when filtering the MB solution. This reduction is due to the presence of the solute, which can obstruct the membrane pores and reduce overall flux.

21967350, 0, Downloaded from https://advanced.onlinelibrary.wiley.com/doi/10.1002/admi.202500888 by National Institutes Of Health Malaysia, Wiley Online Library on [06/04/2026]. See the Terms and Conditions (https://onlinelibrary.wiley.com/terms-and-conditions) on Wiley Online Library for rules of use; OA articles are governed by the applicable Creative Commons License

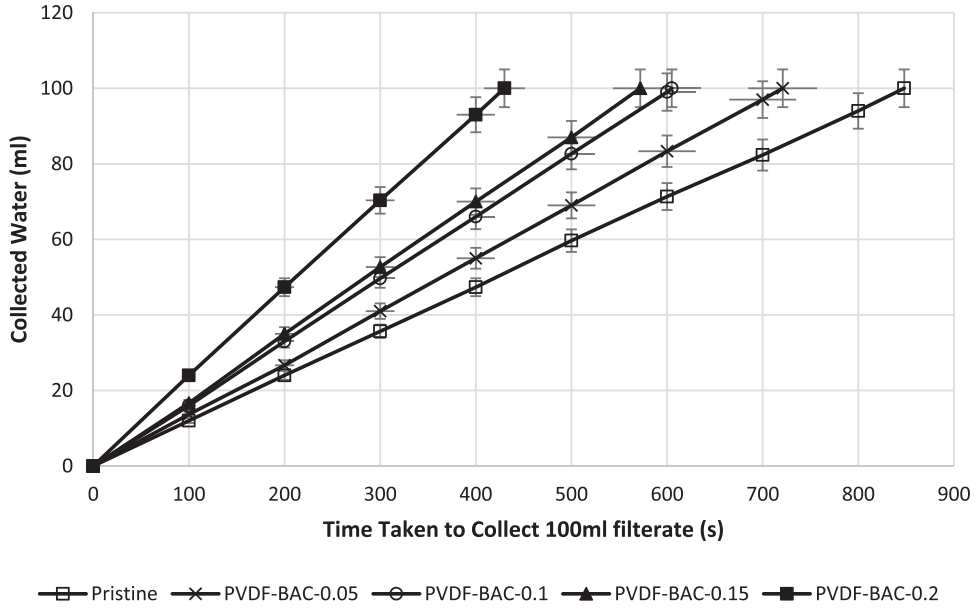

FIGURE 4 | Time interval for pure water collection of pristine and modified membranes.

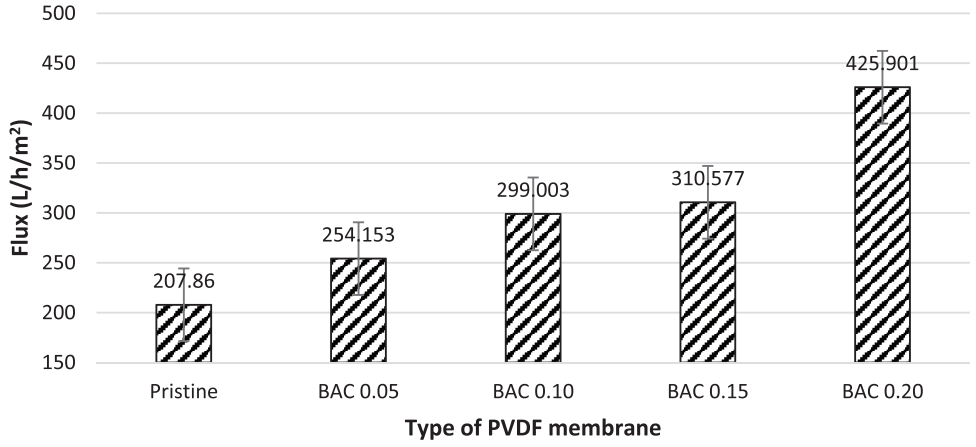

FIGURE 5 | Pure water flux of pristine and modified membranes.

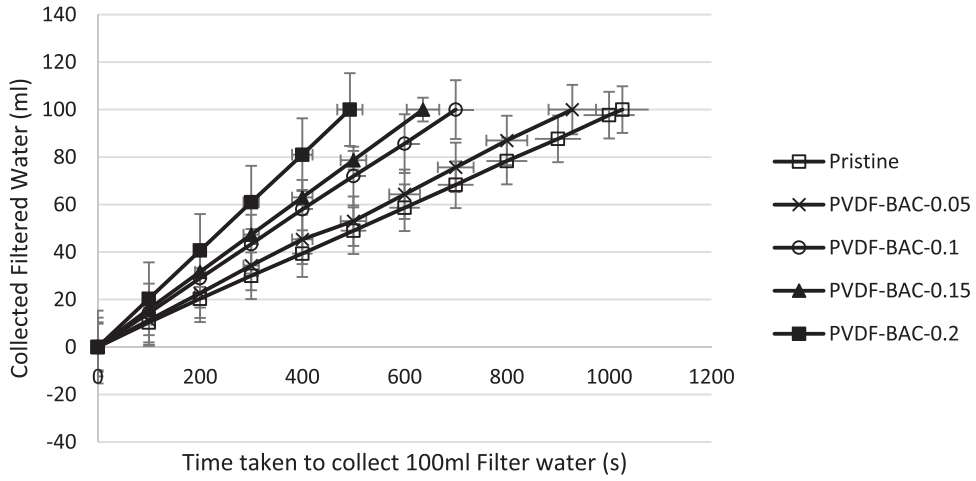

FIGURE 6 | Time interval for 10 mg/L MB solute collection.

21967350, 0, Downloaded from https://advanced.onlinelibrary.wiley.com/doi/10.1002/admi.202500888 by National Institutes Of Health Malaysia, Wiley Online Library on [06/04/2026]. See the Terms and Conditions (https://onlinelibrary.wiley.com/terms-and-conditions) on Wiley Online Library for rules of use; OA articles are governed by the applicable Creative Commons License

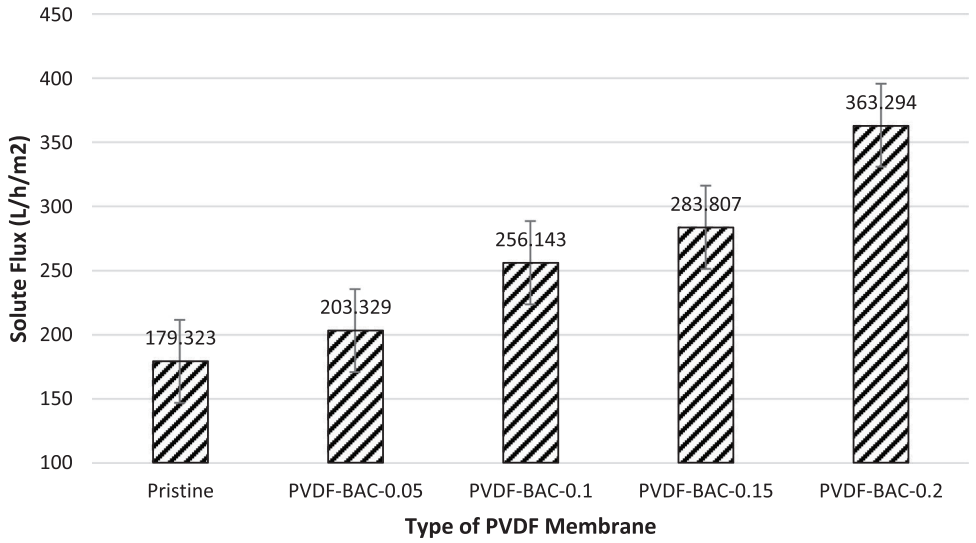

FIGURE 7 | Comparison of solute flux across different membrane types.

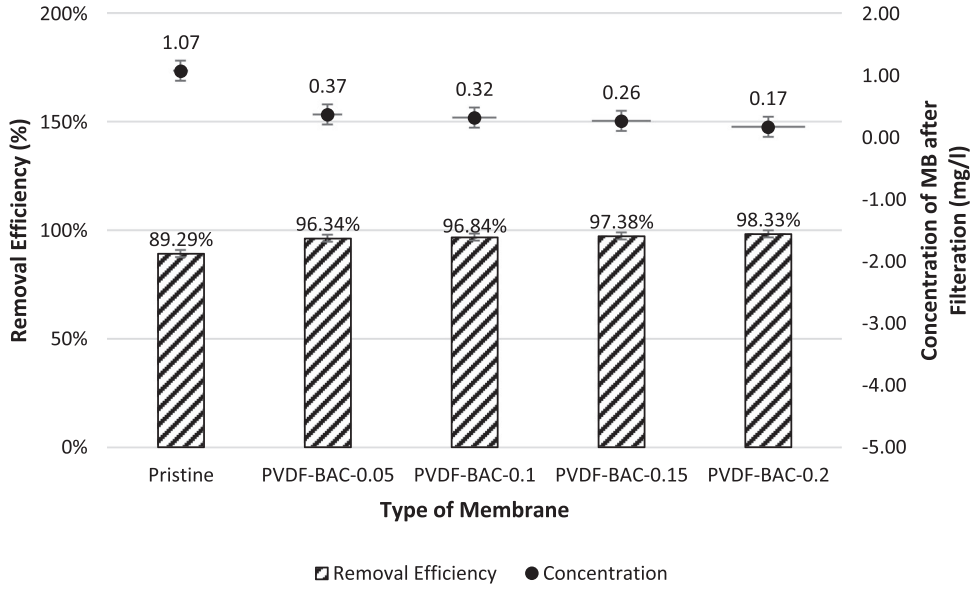

FIGURE 8 | Methylene blue (MB) concentration and removal efficiency of the membrane at an initial MB concentration of 10 mg/L.

3.5 | Rejection of Methylene Blue (MB)

The effects of the initial concentration of 10 mg/L methylene blue on equilibrium concentration, adsorption capacity, and removal efficiency were analyzed and presented in Figure 8. The pristine membrane exhibited an MB concentration of 1.07 mg/L at equilibrium, yielding a removal efficiency of 89.29%. The performance of PVDF membranes was dramatically enhanced when they were modified with varied quantities of biomass-activated carbon (BAC). The PVDF-BAC-0.05 membrane diminished the MB content to 0.37 mg/L, exhibiting an adsorption capacity of 19.27 mg/g and enhancing the removal effectiveness to 96.34%. This demonstrated that at a modest concentration of BAC, the membrane attained considerable adsorption, decreasing the MB concentration considerably from 10 mg/L to 0.37 ppm. PVDF-BAC-0.1 has an adsorption capacity of 9.68 mg/g, resulting in a reduction of the filtered MB concentration to 0.32 mg/L, with a removal efficiency of 96.84%. This indicated a decrease in adsorption ability relative to PVDF-BAC-0.05; it still efficiently decreased the MB content. The trend persisted with PVDF-BAC-0.15 and PVDF-BAC-0.2 membranes, exhibiting MB concentrations of 0.26 and 0.17 mg/L, with removal efficiency of 97.38% and 98.33%, respectively. An increased BAC content may diminish the adsorption capacity per gram while simultaneously enhancing the overall efficacy of the membrane in decreasing MB concentration. This resulted from the enhanced dispersion and interaction with BAC within the membrane matrix, facilitating more efficient adsorption sites and superior overall efficiency in eliminating MB from the solution.

The removal efficiency is significantly influenced by the initial concentration of the adsorbate solution. To assess the impact

21967350, 0, Downloaded from https://advanced.onlinelibrary.wiley.com/doi/10.1002/admi.202500888 by National Institutes Of Health Malaysia, Wiley Online Library on [06/04/2026]. See the Terms and Conditions (https://onlinelibrary.wiley.com/terms-and-conditions) on Wiley Online Library for rules of use; OA articles are governed by the applicable Creative Commons License

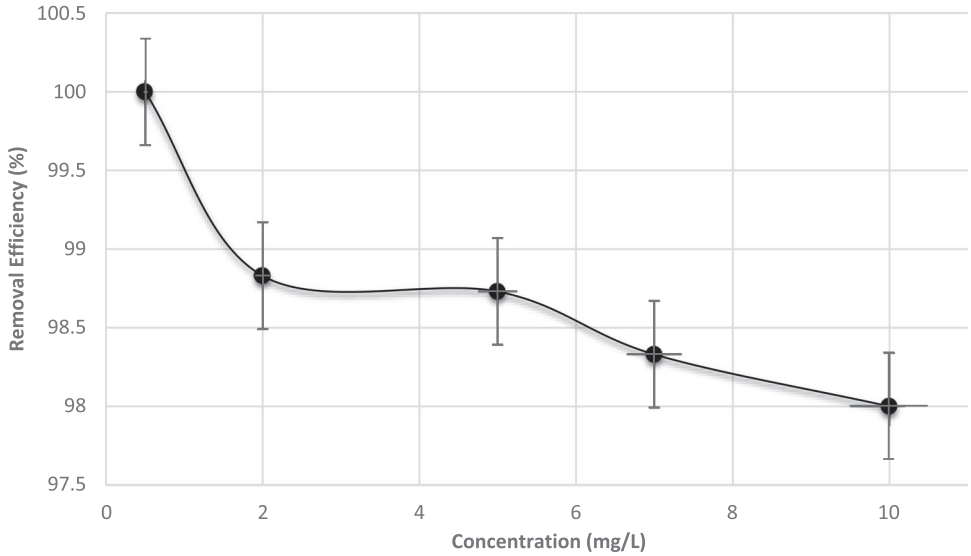

FIGURE 9 | Effect of initial concentration on the removal of MB by PVDF-BAC-0.2.

of primary concentration, 50 mL solutions with beginning concentrations ranging from 0.5 to 10 mg/L were processed using the PVDF membrane. Figure 9 illustrates that the removal effectiveness diminishes with increasing initial concentrations, even as the total build-up of methylene blue escalates.

The overall accumulation of methylene blue escalated with increasing initial concentrations, presumably due to enhanced interaction between the adsorbent sites and MB molecules (Rahman, Amin, & Alam, 2012). Nonetheless, the removal efficiency diminishes when the adsorbate concentration in the solution escalates. The experiment demonstrated that nearly 100% of MB was removed at an initial concentration of 0.5 mg/L. At low concentrations, most of the methylene blue in the sample solution may interact with the active sites of the adsorbent. As the concentration rises, not all MB species can interact with the active surface due to the saturation of available sites, as noted by Rahman, Amin & Alam (2012). This elucidates the inverse correlation between initial concentration and removal efficiency noted in the experiment.

3.6 | Mass Transfer Kinetic

The objectives of modelling are to create mathematical instruments that facilitate the integration of knowledge related to the phenomena of global ($[kLa]_g$), external ($[kLa]_f$), and internal mass transfer ($[kLa]_d$). The modified mass transfer models that were proposed in the current study have the broadest applicability in determining the resistance of mass transfer for the adsorption of solutes onto the adsorbent in a membrane from synthetic dye water. Figure 10 shows linear regression analysis of the graphing of ln(q) versus ln(t).

The objectives of modelling are to create mathematical instruments that facilitate the integration of knowledge related to the phenomena of global ($[kLa]_g$), external ($[kLa]_f$), and internal mass transfer ($[kLa]_d$). The modified mass transfer models that were proposed in the current study have the broadest applicability in determining the resistance of mass transfer for the adsorption of solutes onto the adsorbent in a membrane from synthetic dye water. Experimental results (Figures 11 and 12) show a consistent representation of the mass transfer factors, demonstrating that all curves [kLa]f are convex and all curves [kLa]d and [kLa]g are concave. The concave [kLa]d and [kLa]g curves indicate that the rate of film mass transfer increases until it reaches an optimum, and then it stabilizes.

On the other hand, the convex [kLa]f curve implies that the diffusion rate in a porous medium decreases, reaches a minimum, and is subsequently stabilized. It is expected that the solute mobility will be impeded by interspecific competition among the solutes in the water sample, resulting in a longer time for the solute to reach the outer surface of the adsorbent than through its diffusion in the pore. A high specific capacitance is the result of the monolithic electrode of the adsorbent, which has a high surface area, and is responsible for the rapid diffusion of solute molecules in the pore [19].

To evaluate global mass transfer, it is crucial to calculate [kLa]g values in accordance with Equation (7), as the variability of the curve trend is significant. The curve [kLa]g demonstrates a progressive transition from a low to high mass transfer potential, culminating in a steady value when the adsorbent in the membrane reaches saturation. The adsorption process continues to exist after the maximum breakpoint, even though the variation of [kLa]d increases in tandem with the reduction in [kLa]f. This would be the case regardless of the progressive increase in the rate of global mass transfer. Current speculation suggests that a repulsive force, likely in the form of the "negative [kLa]f value," is present. This force is analogous to the ionic repulsion force between the adsorbate and acceptor sites, which is greater than the attractive van der Waals force when ions of the same charge are in contact. The breakthrough curve is represented by the modified mass transfer models, which are then applied to the experimental data to ascertain that the resistance of mass transfer is contingent upon the porous diffusion [20].

21967350, 0, Downloaded from https://advanced.onlinelibrary.wiley.com/doi/10.1002/admi.202500888 by National Institutes Of Health Malaysia, Wiley Online Library on [06/04/2026]. See the Terms and Conditions (https://onlinelibrary.wiley.com/terms-and-conditions) on Wiley Online Library for rules of use; OA articles are governed by the applicable Creative Commons License

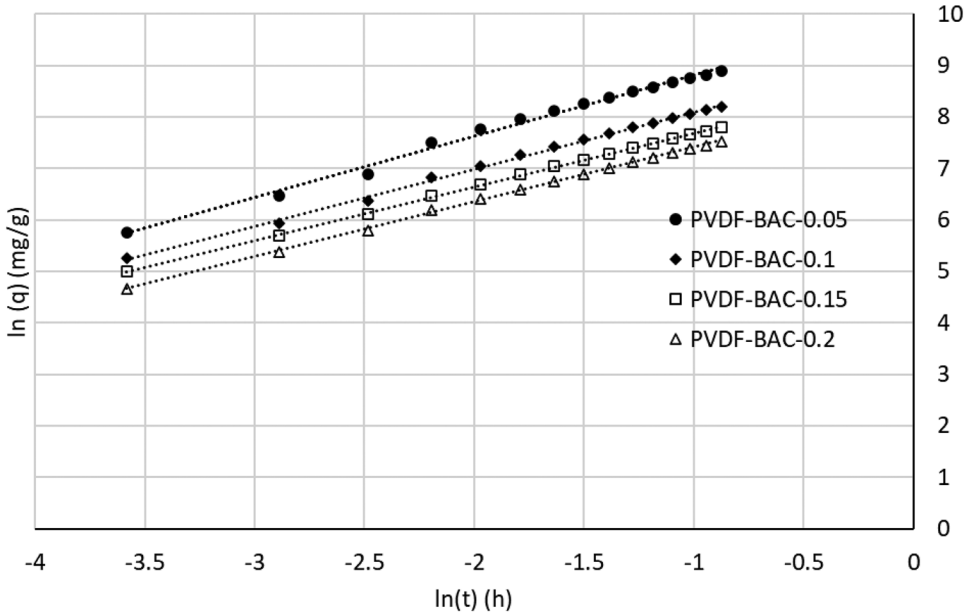

FIGURE 10 | Linear regression analysis of ln(q) versus ln(t) used to verify the β and B parameters applied in the calculation of the apparent mass transfer coefficients $[k_L a]_d$, $[k_L a]_f$, and $[k_L a]_g$over the experimental time range.

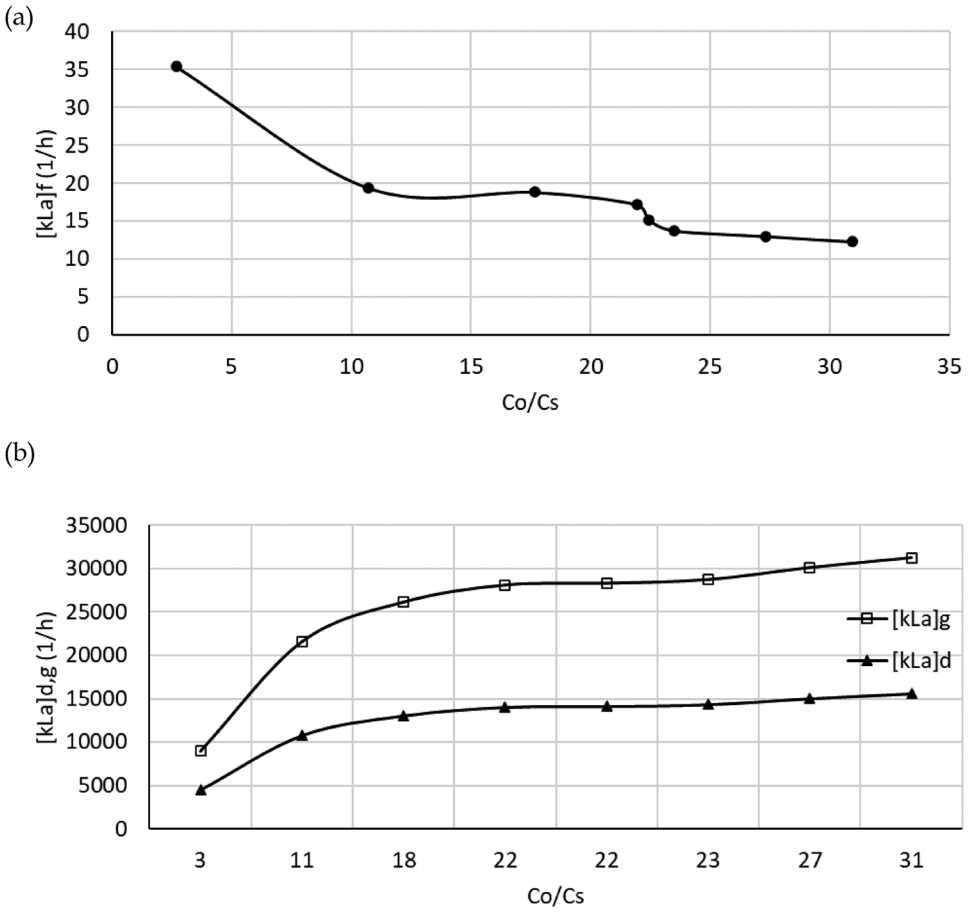

FIGURE 11 | Mass transfer kinetics of methylene blue adsorption from synthetic solution onto the PVDF–BAC-0.05 membrane, analyzed using (a) the film mass transfer coefficient $[k_L a]_f$and (b) the diffusion and global mass transfer coefficients $[k_L a]_{d,g}$as functions of C_0/C_s.

21967350, 0, Downloaded from https://advanced.onlinelibrary.wiley.com/doi/10.1002/admi.202500888 by National Institutes Of Health Malaysia, Wiley Online Library on [06/04/2026]. See the Terms and Conditions (https://onlinelibrary.wiley.com/terms-and-conditions) on Wiley Online Library for rules of use; OA articles are governed by the applicable Creative Commons License

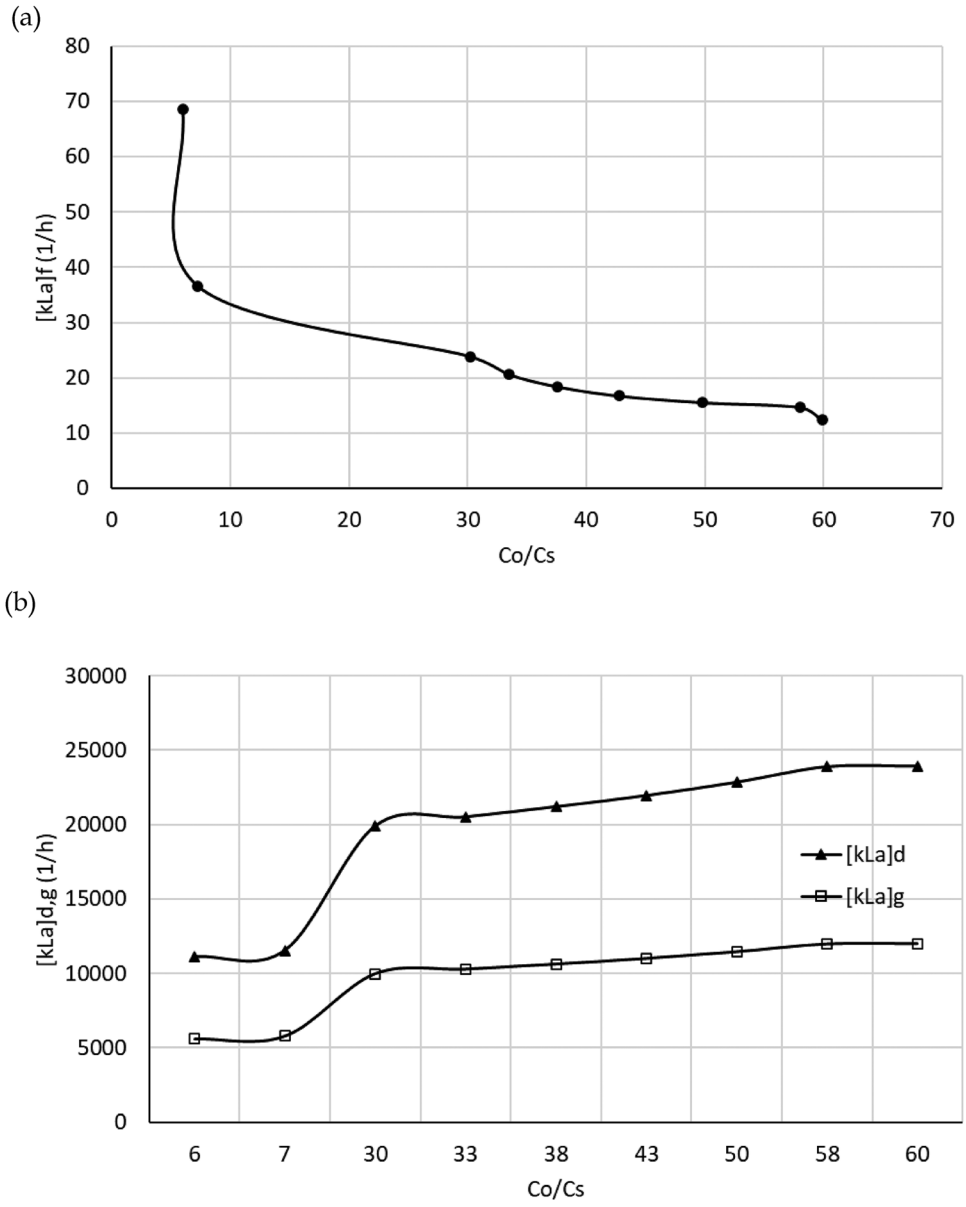

FIGURE 12 | Evaluation of mass transfer kinetics during methylene blue adsorption onto PVDF–BAC-0.2 using (a) film mass transfer coefficient $[k_L a]_f$and (b) diffusion and global mass transfer coefficients $[k_L a]_{d,g}$, plotted against C_0/C_s.

The effects of concentration, granular size distribution, and hydrodynamic conditions, as well as the adsorption of the solute onto the adsorbent in aqueous solution, can be used to define the film mass transfer using the models proposed in a previous study by Chatzopoulos et al. [21]. The granular size distribution of the adsorbent can be analyzed in order to determine the impact of the granular size distribution on the film mass transfer, as the interactive forces between the adsorbate and adsorbent are related to physisorption. This is particularly relevant when non-(less) polar adsorbate molecules are used in the experiments [21]. When a high granular size distribution adsorbent is employed in the adsorption process, the transport of non-(less) polar adsorbate molecules from the bulk liquid to the film zone is more efficient. The film mass transfer is influenced by the extent of the surface area of the adsorbent that captures the adsorbate molecules [22]. Surface area occupation was examined in relation to the adsorption of dye onto biomass-activated carbon in this investigation to determine its impact on film mass transfer. The adsorbent's extensive open surface area facilitates the rapid migration of adsorbate molecules from the bulk solution (C) to the film zone, as evidenced by the rapid decrease in [kLa]f. The adsorbate concentration in the film zone (C*) is minimal, which leads to a significant concentration in the driving force of mass transfer (C-C*).

Consequently, the film mass transfer does not affect the resistance to mass transfer. Because an increase in the occupied BAC surface area leads to an increase in C*, the variation of [kLa]f can continue to decrease progressively. It is essential to ascertain whether film mass transfer is implicated in the regulation of mass transfer resistance. The concentration of C-C* increases in proportion to the concentration of C in the bulk solution, a fact that is widely recognized. To investigate the influence of C on the film mass transfer for the adsorption of dye onto BAC from aqueous

21967350, 0, Downloaded from https://advanced.onlinelibrary.wiley.com/doi/10.1002/admi.202500888 by National Institutes Of Health Malaysia, Wiley Online Library on [06/04/2026]. See the Terms and Conditions (https://onlinelibrary.wiley.com/terms-and-conditions) on Wiley Online Library for rules of use; OA articles are governed by the applicable Creative Commons License

solution, the mathematical models that Chatzopolous et al. [21] had previously proposed were implemented. According to the findings of this investigation, the rate of film mass transmission increases as C increases. The activated carbon used in this study exhibited a specific surface area of 532 m^2 g^{-1}, which is lower than that reported for some waste-derived carbon nanomaterials, such as alkali-activated herbaceous biomass (1368 m^2 g^{-1}) (Osman et al., 2020). This difference can be attributed to variations in precursor type, activation strategy, and pore development. Nevertheless, the surface area obtained in the present study is sufficient to enhance adsorption performance in the composite membrane, while future work may explore the incorporation of waste-derived activated carbon to improve both surface area and sustainability.

4 | Conclusion

The study analyzed the effects of an initial concentration of 10 ppm methylene blue on equilibrium concentration, adsorption capacity, and removal efficiency of PVDF membranes. The pristine membrane showed an MB concentration of 1.07 mg/L, yielding a removal efficiency of 89.29%. PVDF membranes significantly improved when changed with biomass-activated carbon (BAC). PVDF-BAC-0.05 membrane diminished MB content to 0.37 mg/L, enhancing removal effectiveness to 96.34%. PVDF-BAC-0.1 showed a decrease in adsorption ability, but still efficiently decreased MB content. PVDF-BAC-0.2 membrane demonstrated the lowest concentration of MB after filtration. The initial concentration of the adsorbate solution has a substantial impact on the removal efficacy. The experiment illustrated that an initial concentration of 0.5 mg/L resulted in the removal of nearly 100% methylene blue. In determining the resistance of mass transfer for the adsorption process, the modified mass transfer models proposed in this study have the broadest applicability. The experimental results indicate that all curves [kLa]f are convex, while all curves [kLa]d and [kLa]g are concave. The concave [kLa]d and [kLa]g curves indicate that the rate of film mass transfer increases, reaches a maximum, and stabilizes. The study also investigates the influence of surface area occupation on the mass transfer of the film in relation to the adsorption of dye onto biomass-activated carbon. This rapid decrease in [kLa]f suggests that the adsorbate molecules are migrating rapidly from the bulk solution (C) to the film zone, a process that is facilitated by the extensive adsorbent open surface area. The resistance to mass transfer is not influenced by the film mass transfer as the concentration of C-C* increases in conjunction with the concentration of C in the bulk solution. The significance of comprehending the role of surface area occupation in regulating the resistance of mass transfer in the adsorption process is underscored by the fact that the film mass transfer rate increases as C increases.

Author Contributions

K.A.M.S. contributed to writing (original draft, review, and editing), methodology, investigation, data curation, formal analysis, validation, conceptualization, and visualization. S.A. to methodology, data curation, investigation, and writing (review and editing). S.Z.M.A. to methodology, investigation, and data curation. K.A.M.S. to supervision, resources, project administration, and writing (review and editing). H.R.R. and M.R.R. to methodology, investigation, and data curation. I.Y. to supervision, resources, project administration, funding acquisition, conceptualization, and writing (review and editing).

Acknowledgment

The authors would like to acknowledge Universiti Malaysia Sarawak (UNIMAS) for financial support through the Mentor Grant (UNI/F02/MENTOR/86086/2023). The author is also grateful for the support given throughout this research, especially to Mr. Airul Azhar Bin Jitai and Miss Dayang Fadhilatul Aishah Abang Abdul Hamid.

Conflicts of Interest

The authors declare no conflicts of interest.

Data Availability Statement

The data that support the findings of this study are available from the corresponding author upon reasonable request.

References

1. S. Rafaqat, N. Ali, C. Torres, and B. Rittmann, "Recent Progress in Treatment of Dyes Wastewater Using Microbial-electro-Fenton Technology," *RSC Advances* 12 (2022): 17104–17137, https://doi.org/10.1039/d2ra01831d.

2. J. Fito, M. Abewaa, A. Mengistu, et al., "Adsorption of Methylene Blue From Textile Industrial Wastewater Using Activated Carbon Developed From Rumex abyssinicus Plant," *Scientific Reports* 13, no. 1 (2023): 5427, https://doi.org/10.1038/s41598-023-32341-w.

3. P. O. Oladoye, T. O. Ajiboye, E. O. Omotola, and O. J. Oyewola, "Methylene Blue Dye: Toxicity and Potential Elimination Technology From Wastewater," *Results in Engineering* 16 (2022): 100678, https://doi.org/10.1016/j.rineng.2022.100678.

4. K. A. M. Said, C. Sari, and M. R. Rahman, "Membranes for the Removal of Endocrine Disrupting Compounds From Aqueous Environments," *Advanced Materials for Emerging Water Pollutant Removal*, edited by P. S. Goh, D. Kanakaraju, A. Iqbal, and A. F. Ismail, (Royal Society of Chemistry, 2024), https://doi.org/10.1039/9781837675425-00052.

5. J. Lin, W. Ye, M.-C. Baltaru, et al., "Tight Ultrafiltration Membranes for Enhanced Separation of Dyes and Na_2SO_4 During Textile Wastewater Treatment," *Journal of Membrane Science* 514 (2016): 217–228, https://doi.org/10.1016/j.memsci.2016.04.057.

6. J. M. Dias, M. C. M. Alvim-Ferraz, M. F. Almeida, J. Rivera-Utrilla, and M. Sánchez-Polo, "Waste Materials for Activated Carbon Preparation and Its Use in Aqueous-phase Treatment: A Review," *Journal of Environmental Management* 85, no. 4 (2007): 833–846, https://doi.org/10.1016/j.jenvman.2007.07.031.

7. Z.-Q. Huang and Z.-F. Cheng, "Recent Advances in Adsorptive Membranes for Removal of Harmful Cations," *Journal of Applied Polymer Science* 137, no. 13 (2020): 48579, https://doi.org/10.1002/app.48579.

8. W. C. Chong, Y. L. Choo, C. H. Koo, Y. L. Pang, and S. O. Lai, "Adsorptive Membranes for Heavy Metal Removal–A Mini Review," *AIP Conference Proceedings* 2157, no. 1 (2019): 020005, https://doi.org/10.1063/1.5126540.

9. M. R. Adam, S. K. Hubadillah, and M. I. M. Esham, "Chapter 12-Adsorptive Membranes for Heavy Metals Removal From Water," *Membrane Separation Principles and Applications*, edited by A. F. Ismail, M. A. Rahman, M. H. D. Othman, and T. Matsuura, (Elsevier, 2019): 361–400, https://doi.org/10.1016/B978-0-12-812815-2.00012-0.

10. E. Salehi, P. Daraei, and A. Arabi Shamsabadi, "A Review on Chitosan-Based Adsorptive Membranes," *Carbohydrate Polymers* 152 (2016): 419–432, https://doi.org/10.1016/j.carbpol.2016.07.033.

11. S. Balta, A. Sotto, P. Luis, L. Benea, B. Van der Bruggen, and J. Kim, "A New Outlook on Membrane Enhancement With Nanoparticles: The

21967350, 0, Downloaded from https://advanced.onlinelibrary.wiley.com/doi/10.1002/admi.202500888 by National Institutes Of Health Malaysia, Wiley Online Library on [06/04/2026]. See the Terms and Conditions (https://onlinelibrary.wiley.com/terms-and-conditions) on Wiley Online Library for rules of use; OA articles are governed by the applicable Creative Commons License

Alternative of ZnO," *Journal of Membrane Science* 389 (2012): 155–161, https://doi.org/10.1016/j.memsci.2011.10.025.

12. S. Zinadini, A. A. Zinatizadeh, M. Rahimi, V. Vatanpour, and H. Zangeneh, "Preparation of a Novel Antifouling Mixed Matrix PES Membrane by Embedding Graphene Oxide Nanoplates," *Journal of Membrane Science* 453 (2014): 292–301, https://doi.org/10.1016/j.memsci.2013.10.070.

13. D. Qadir, H. Mukhtar, and L. K. Keong, "Mixed Matrix Membranes for Water Purification Applications," *Separation & Purification Reviews* 46, no. 1 (2017): 62–80, https://doi.org/10.1080/15422119.2016.1196460.

14. O. Lytken, W. Lew, and C. T. Campbell, "Catalytic Reaction Energetics by Single Crystal Adsorption Calorimetry: Hydrocarbons on Pt(111)," *Chemical Society Reviews* 37, no. 10 (2008): 2172–2179, https://doi.org/10.1039/B719543P.

15. L. Schimka, J. Harl, A. Stroppa, et al., "Accurate Surface and Adsorption Energies From Many-Body Perturbation Theory," *Nature Materials* 9, no. 9 (2010): 741–744, https://doi.org/10.1038/nmat2806.

16. M. A. Fulazzaky, "Determining the Resistance of Mass Transfer for Adsorption of the Surfactants Onto Granular Activated Carbons From Hydrodynamic Column," *Chemical Engineering Journal* 166, no. 3 (2011): 832–840, https://doi.org/10.1016/j.cej.2010.11.052.

17. M. A. Fulazzaky, "Analysis of Global and Sequential Mass Transfers for the Adsorption of Atrazine and Simazine Onto Granular Activated Carbons From a Hydrodynamic Column," *Analytical Methods* 4, no. 8 (2012): 2396–2403, https://doi.org/10.1039/C2AY05467A.

18. Z. Li, X. Luo, and Y. Li, "Reed Rhizome Residue-Based Activated Carbon Adsorption Ultrafiltration Membranes for Enhanced MB Removal," *ACS Omega* 7, no. 48 (2022): 43829–43838, https://doi.org/10.1021/acsomega.2c04968.

19. G. Hasegawa, M. Aoki, K. Kanamori, K. Nakanishi, T. Hanada, and K. Tadanaga, "Monolithic Electrode for Electric Double-layer Capacitors Based on Macro/Meso/Microporous S-Containing Activated Carbon With High Surface Area," *Journal of Materials Chemistry* 21, no. 7 (2011): 2060–2063, https://doi.org/10.1039/C0JM03793A.

20. T. J. Giesy and M. D. LeVan, "Mass Transfer Rates of Oxygen, Nitrogen, and Argon in Carbon Molecular Sieves Determined by Pressure-swing Frequency Response," *Chemical Engineering Science* 90 (2013): 250–257, https://doi.org/10.1016/j.ces.2012.12.029.

21. D. Chatzopoulos, A. Varma, and R. L. Irvine, "Adsorption and Desorption Studies in the Aqueous Phase for the Toluene/Activated Carbon System," *Environmental Progress* 13 (1994): 21–25, https://doi.org/10.1002/ep.670130113.

22. V. Meshko, L. Markovska, M. Mincheva, and A. E. Rodrigues, "Adsorption of Basic Dyes on Granular Acivated Carbon and Natural Zeolite," *Water Research* 35, no. 14 (2001): 3357–3366, https://doi.org/10.1016/S0043-1354(01)00056-2.

Supporting Information

Additional supporting information can be found online in the Supporting Information section.

Supporting File: admi70480-sup-0001-SuppMat.docx.

21967350, 0, Downloaded from https://advanced.onlinelibrary.wiley.com/doi/10.1002/admi.202500888 by National Institutes Of Health Malaysia, Wiley Online Library on [06/04/2026]. See the Terms and Conditions (https://onlinelibrary.wiley.com/terms-and-conditions) on Wiley Online Library for rules of use; OA articles are governed by the applicable Creative Commons License